




Rationalizing doping and electronic correlations in LaFe_2As_2 Tommaso Gorni , Diego Florez-Ablan , and Luca de' Medici *LPEM, ESPCI Paris, PSL Research University, CNRS, Sorbonne Université, 75005 Paris, France*

(Received 17 October 2022; revised 27 February 2023; accepted 15 March 2023; published 31 March 2023)

We compute the electronic properties of the normal state of uncollapsed LaFe_2As_2 , taking into account local dynamical correlations by means of slave-spin mean-field+density-functional theory. Assuming the same local interaction strength used to model the whole electron- and hole-doped BaFe_2As_2 family, our calculations reproduce the experimental Sommerfeld specific heat coefficient, which is twice the value predicted by uncorrelated band theory. We find that LaFe_2As_2 has a reduced bare bandwidth and this solves the apparent paradox of its sizable correlations despite its nominal valence $d^{6.5}$, which would imply extreme overdoping and uncorrelated behavior in BaFe_2As_2 . Our results yield a consistent picture of the whole 122 family and point at the importance of the correlation strength, rather than sheer doping, in the interpretation of the phase diagram of iron-based superconductors

DOI: [10.1103/PhysRevB.107.125166](https://doi.org/10.1103/PhysRevB.107.125166)**I. INTRODUCTION**

The conventional phase diagram of iron-based superconductors (IBSC) typically displays three zones: the paramagnetic metallic parent compound, an antiferromagnetic metal obtained upon lowering the temperature, and a superconducting phase replacing the magnetic order upon (both electron- and hole-) doping or under pressure [1–3]. Excluding the notable exceptions of, e.g., FeSe and LiFeAs (which lack the magnetic phase), such a phase diagram is shared among different IBSC families [1–5], and it has been thoroughly studied in the 122 family by leveraging on the ease at doping the BaFe_2As_2 parent compound with holes in the $\text{Ba}_{1-x}\text{K}_x\text{Fe}_2\text{As}_2$ series, and with electrons in the $\text{Ba}(\text{Fe}_{1-x}\text{Co}_x)_2\text{As}_2$ series [6,7]. These studies gave evidence of a strong asymmetry between the hole- and electron-doped side; in the former, the superconducting dome extends up to 0.5–0.6 extra holes per unit cell, while in the latter the superconducting critical temperature (T_c) drops down to zero before reaching 0.15 extra electrons per Fe atom [2,3].

Recent studies on the (uncollapsed) $\text{La}_{0.5-x}\text{Na}_{0.5+x}\text{Fe}_2\text{As}_2$ series, where hole and electron doping are attained by acting only on the intercalated layer, initially showed similar results on the hole-doped ($x > 0$) side, where a superconducting phase emerges from an antiferromagnetic state around $x \approx 0.15$ and reaches the maximum $T_c = 27.0$ k at $x \approx 0.3$ [8]. The later discovery of superconductivity in the electron-doped end member of the series, LaFe_2As_2 , with $T_c \approx 12.1$ k, therefore, came as a surprise; the compound corresponding to a nominal valence of 6.5 electrons for the Fe ion [9], i.e., a doping of 0.5 electrons from the valence of the reference parent, compounds in all iron-based superconductors, like BaFe_2As_2 . There, at this extreme electron overdoping, superconductivity has long disappeared.

Such a finding has been initially explained via band-structure analysis by means of DFT (GGA) calculations, showing that the strong hybridization between the La-5*d* and the Fe-3*d* levels conceals a hole pocket generated by Fe

bands, suggesting a smaller electronic doping, estimated in the range of 0.25–0.40 e^-/Fe [10,11]. However, band structures derived from LDA and GGA functionals are known to yield a poor description of electronic quasiparticles in IBSC, mainly due to the underestimation of local dynamical correlations, leading to at least a factor-two discrepancy between the computed and experimental electronic bandwidths [12–16]. Even though these effects are supposed to be less relevant on the electron-doped side, nuclear magnetic and quadrupolar resonance (NMR and NQR) studies found that antiferromagnetic spin fluctuations are not completely suppressed in LaFe_2As_2 [contrary to what happens in $\text{Ba}(\text{Fe}_{0.5}\text{Co}_{0.5})_2\text{As}_2$] [17], and specific heat measurements have shown a Sommerfeld coefficient roughly a factor two bigger than what predicted by DFT (GGA, LDA) calculations [18]. While the first finding alone leaves the door open to an uncorrelated, smaller effective doping scenario, when considered together with the specific heat measurement it points more likely to a decisive role played by electronic correlations in LaFe_2As_2 . More accurate treatments of these dynamical correlation effects by means, e.g., of dynamical mean-field theory (DMFT) or slave-particle approaches, have indeed been shown to generally provide electronic bandwidths in much closer agreement with experimental findings in IBSC, and generally improve the description of their low-energy electronic properties [19–21]. DMFT studies have been performed on LaFe_2As_2 and CaFe_2As_2 compounds in order to inspect the structural and doping dependence of the superconducting transition coming, however, to rather different conclusions, most likely due to the usage of different structural parameters and interaction-strength values [22,23].

Here, we study LaFe_2As_2 electronic properties by deriving a realistic tight-binding from DFT (GGA) calculations, and taking into account local dynamical correlations by means of slave-spin mean-field (SSMF) theory. The numerical agility of our approach allows us to explore the interaction-strength space and pinpoint the interaction value by comparing against recent specific heat measurements [18]. We find that the

TABLE I. Structural parameters of the 122 family used in our numerical simulations, corresponding to the experimental uncollapsed body-centered tetragonal phase. The z_{As} coordinate is reported in units of the c -axis length.

	LaFe ₂ As ₂ [9]	BaFe ₂ As ₂ [27]	KFe ₂ As ₂ [27]
a (Å)	3.9376	3.9625	3.844
c (Å)	11.7317	13.0168	13.916
z_{As}	0.3657	0.3545	0.35249

experimental Sommerfeld coefficient of LaFe₂As₂ is reproduced by using the same interaction values which captures its evolution throughout a large variety of electron- and hole-doped BaFe₂As₂ [7], so placing LaFe₂As₂ in the same theoretical framework of other 122 compounds. We compare the series of stoichiometric compounds XFe₂As₂ with X = K, Ba, La and indeed, correlations decrease drastically with increasing filling (5.5, 6.0, and 6.5 electrons/Fe, respectively), as expected in the scenario positing the influence of a Mott insulator that would be realized at half-filling (i.e., 5.0 electrons/Fe) and extending its influence over a large range of electronic densities [20]. However, further inspection of the model reveals correlations are stronger in LaFe₂As₂ with respect to a simulation of BaFe₂As₂ doped with electrons to reach the same nominal valence of 6.5 electrons, mainly due to the smaller bare bandwidth of the former. Therefore, we argue that the apparent paradox of superconductivity at high electron doping in LaFe₂As₂ can be solved by analyzing the phase diagram in terms of the strength of local correlations, rather than sheer doping.

II. DFT CALCULATIONS

The DFT calculations with the PBE functional have been carried out with the QUANTUM ESPRESSO package [24,25], using norm-conserving pseudopotentials from the PseudoDojo library [26] and a plane-wave cutoff of $\epsilon_{\text{cut}} = 90$ Ry. Integrals over the Brillouin zone have been converged with a gaussian smearing of $\sigma = 0.01$ Ry and a Γ -centred Monkhorst-Pack grid of $8 \times 8 \times 8$ points. The crystal structures have been fixed to the experimental values, resumed in Table I.

The PBE density of states (DoS) of LaFe₂As₂, BaFe₂As₂, and KFe₂As₂ are reported in Fig. 1, together with their projections onto the Fe-3*d* and As-4*p* atomic wave functions [28]. The DoS profiles show the typical structure of IBSC compounds, with low-energy quasiparticles, mainly of Fe-3*d* character mildly hybridized with the subjacent As-4*p* bands, and are consistent with a hole-doping of the Fe3*d* manifold proceeding from LaFe₂As₂ to KFe₂As₂, passing through BaFe₂As₂. We further notice that the Fe3*d* manifold roughly starts around -2 eV in all the three compounds, but has different extensions within the empty-state manifold. While in KFe₂As₂, the Fe3*d* manifold has negligible hybridization with the above empty K-3*d* bands; it hybridizes with the Ba-5*d* empty bands in BaFe₂As₂, and with the La-5*d* bands in LaFe₂As₂ (conversely, the localized La-4*f* electrons, yielding the narrow peak in the DoS around 2 eV, have negligible hybridization with the conduction manifold). This results into

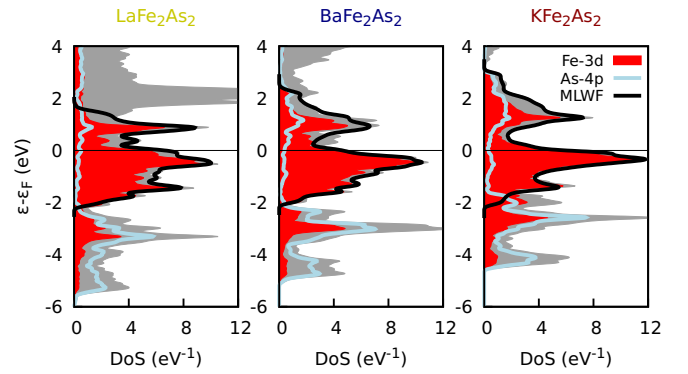


FIG. 1. PBE density of states (DoS) per unit cell of the 122 compounds (gray). The PBE DoS projected on Fe-3*d* atomic states is shown in red, while the DoS projected on the As-4*p* atomic states is shown in light blue. The black line represents the DoS obtained by our maximally Wannier function (MLWF) construction spanning the low-energy region around the Fermi level.

different conduction bandwidths at the PBE level, which, as it appears from their projections on the Fe-3*d* wave functions, decreases going from KFe₂As₂ to BaFe₂As₂, and from BaFe₂As₂ to LaFe₂As₂.

A relevant quantity that can be extracted from the value of the DoS at the Fermi level is the Sommerfeld coefficient $\gamma_n = \pi^2 k_B^2 \text{DoS}(\epsilon_F)/3$, i.e., the linear coefficient in the electronic specific heat as a function of temperature, which is a sensitive probe of the renormalized band structure and thus, of local dynamical correlations. As it has been previously shown, the γ_n coefficients computed at the PBE level tend to be smaller than the experimental values in the whole 122 family, with mass enhancements ranging from $\gamma_n^{\text{exp.}}/\gamma_n^{\text{PBE}} \approx 1.2$ for electron dopings of 0.2, up to $\gamma_n^{\text{exp.}}/\gamma_n^{\text{PBE}} \approx 10$ for hole dopings of 0.5 realized, i.e., in KFe₂As₂ [7,20]. In the case of LaFe₂As₂, our calculations yield $\gamma_n^{\text{PBE}} \approx 18$ mJ mol⁻¹k⁻², to be compared against the experimental estimate of $\gamma_n^{\text{exp.}} = (35 \pm 2)$ mJ mol⁻¹k⁻² [18]. On one hand, such a factor-two difference testifies the relevant impact of local dynamical correlations but, on the other hand, it does not reconcile with the traditional phase diagram of the 122 family, showing vanishing mass enhancements (and no superconducting transition) for electron doping beyond ≈ 0.2 [6].

III. WANNIER D-MODEL

In order to address the effect of local dynamical correlations, we project the PBE Bloch states spanning the lowenergy manifold on a set of five maximally localized Wannier functions centered on each Fe site, using the WANNIER90 code [30]. Such a procedure is welldefined when applied to a subset of isolated energy bands, however, difficulties may arise when the target Bloch states overlap with other energy bands. In these cases, a disentanglement procedure needs to be applied before proceeding with the spread minimization, i.e., a subset of energy bands has to be chosen for each k point [31]. The typical disentanglement procedure starts from the projection of the Bloch states lying within a larger energy window over a set of trial localized orbitals with a given atomic symmetry,

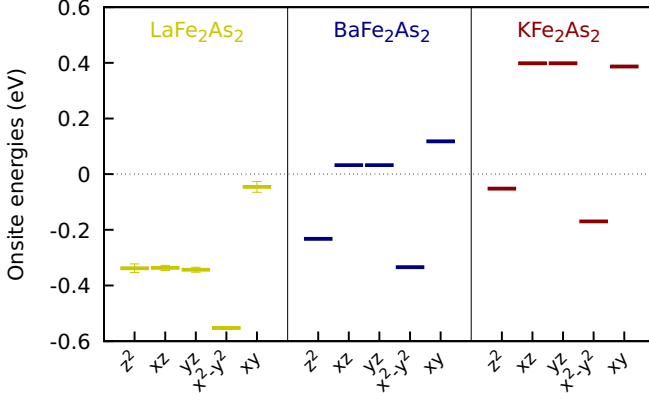


FIG. 2. Onsite energies of our maximallylocalized-Wannier-function d models, referred to the respective Fermi energies. The error bars represent the discrepancy between the two Fe sites, noticeable only in the case of LaFe₂As₂.

and by orthonormalizing the resulting set via the Löwdin procedure. The resulting wave functions can be further refined by imposing smoothness in the k space [32]. In practice, such a procedure is performed only over a subset of the Bloch states, since the one residing in a smaller energy window are kept frozen, in order to enforce the final local basis set to faithfully reproduce the original bands, at the price of less-localized Wannier functions.

In the cases considered here, KFe₂As₂ presents no particular difficulties and the final set of maximallylocalized Wannier functions faithfully describes the conduction manifold. For what concerns BaFe₂As₂, the hybridization with the Ba5 d manifold hampers a proper description of empty bands; nonetheless, a well-behaved set of Wannier functions is reached with the spread minimization [33,34]. Finally, in the case of LaFe₂As₂, these difficulties become severe due to the stronger hybridization with the La-5 d bands, and only Wannier projection models including these states explicitly have been considered in the literature so far [10,11,23].

In the spirit of finding a minimal d model for the conduction bands, we have pursued this path for LaFe₂As₂ by carefully inspecting the quality of the tight-binding Hamiltonian as different disentanglement energy windows were considered. We noticed that, even though the Bloch states are reproduced quite satisfactorily by different d models, the disentanglement procedure breaks the equivalence between the two iron sites. Among these, we have therefore chosen the d model with the minimum difference among the onsite energies of the two equivalent iron atoms, quantified on average as ≈ 0.02 eV and with a maximum deviation of ≈ 0.04 eV in the case of the xy orbital. [34] The resulting onsite levels are shown in Fig. 2 compared with the ones of BaFe₂As₂ and KFe₂As₂, showing an overall consistency within the 122 family and confirming the electron-doped character of the d manifold in LaFe₂As₂. Finally, in Fig. 1 we compare the DoS of our tight-binding models (black lines) with the PBE ones, which validate our preliminary estimates of the d -manifold bandwidths in these compounds yielding $W \approx 5.4$ eV in KFe₂As₂, $W \approx 4.7$ eV in BaFe₂As₂, and $W \approx 4.1$ eV in LaFe₂As₂.

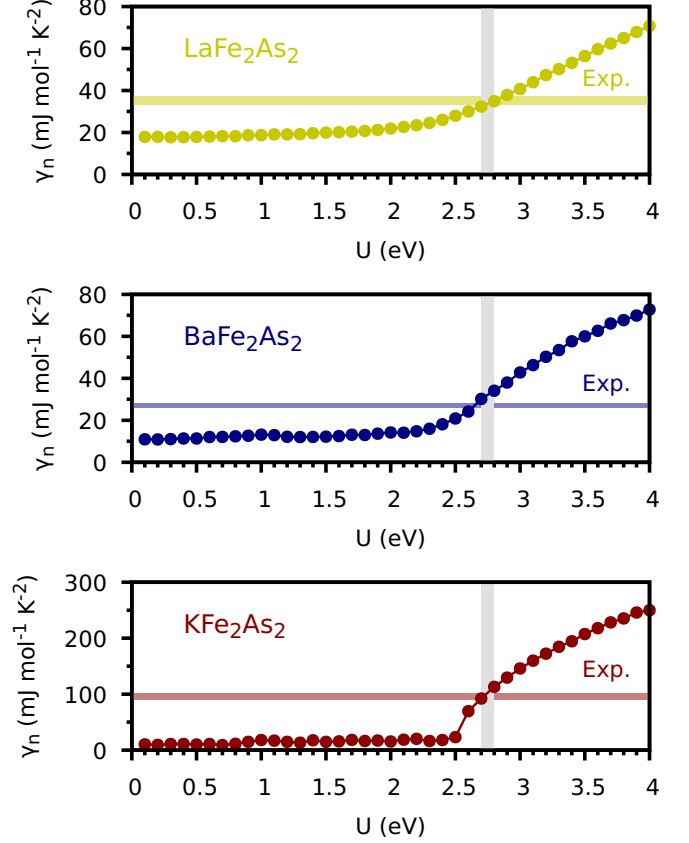


FIG. 3. Sommerfeld coefficients of the 122 family from our SSMF@PBE calculations as a function of the Hubbard U strength ($J/U = 0.25$), compared with the experimental values [7,18]. The trend over the whole family is captured by $U \approx 2.7 - 2.8$ eV (gray line). The $U = 0$ value corresponds to the PBE case.

IV. LOCAL DYNAMICAL CORRELATIONS

The projection of the PBE Bloch states onto maximallylocalized Wannier functions, as discussed in the previous section, yields a tight-binding Hamiltonian in the form of

$$\hat{\mathcal{H}}_0 = \sum_{\substack{i \neq j \\ m, m', \sigma}} t_{ij}^{mm'} \hat{d}_{im\sigma}^\dagger \hat{d}_{jm'\sigma} + \sum_{i, m, \sigma} \epsilon_{im\sigma} \hat{n}_{im\sigma}, \quad (1)$$

where $\hat{d}_{im\sigma}^\dagger$ creates an electron in the Wannier spin-orbital $m\sigma$ and lattice site i , and $\hat{n}_{im\sigma} = \hat{d}_{im\sigma}^\dagger \hat{d}_{im\sigma}$ is the corresponding number operator.

A Hubbard-Kanamori Hamiltonian is used to include the local interactions to be treated in a dynamical many-body fashion:

$$\begin{aligned} \hat{\mathcal{H}} = & \hat{\mathcal{H}}_0 + U \sum_{im} \hat{n}_{im\uparrow} \hat{n}_{im\downarrow} \\ & + (U - 2J) \sum_{i, m \neq m'} \hat{n}_{im\uparrow} \hat{n}_{im'\downarrow} \\ & + (U - 3J) \sum_{i, m < m', \sigma} \hat{n}_{im\sigma} \hat{n}_{im'\sigma}, \end{aligned} \quad (2)$$

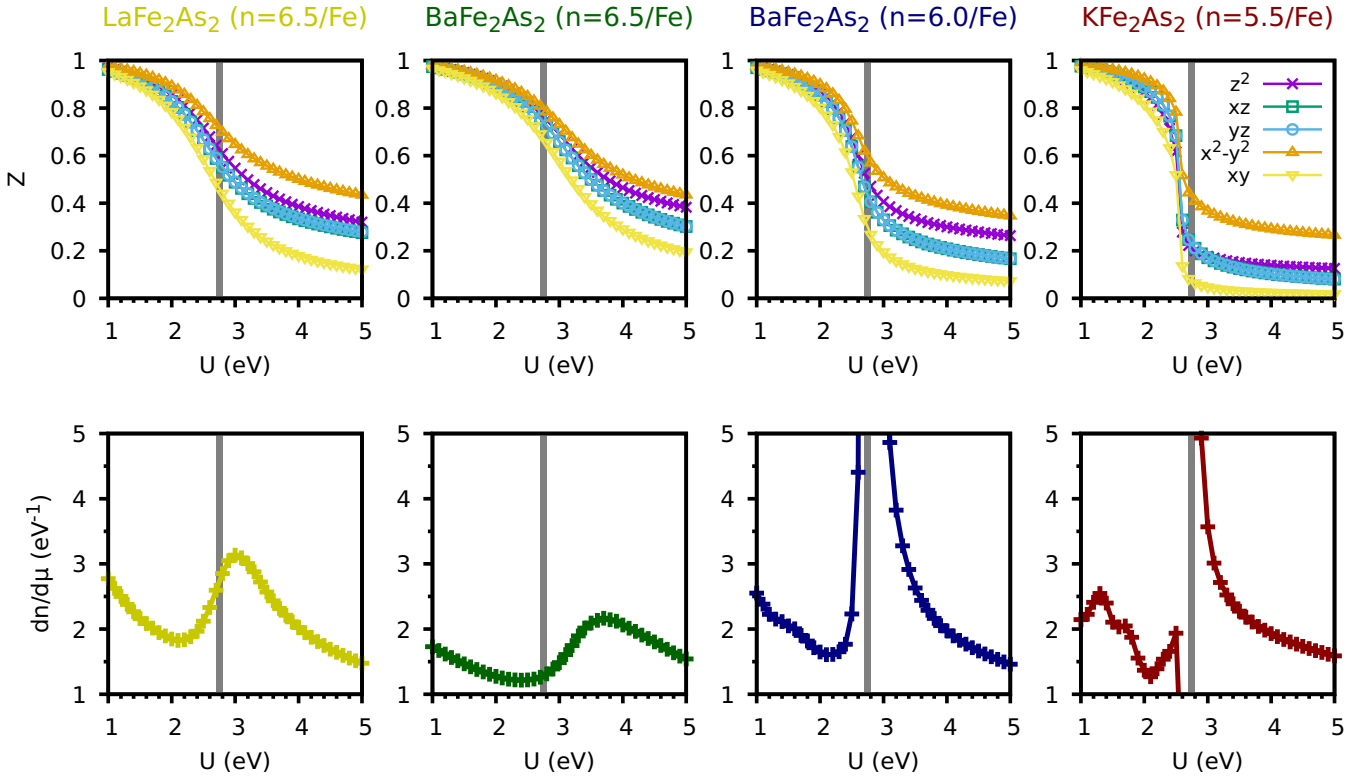


FIG. 4. Top panels: quasiparticle weights Z of 122 family computed within the SSMF@PBE approach as a function of the Hubbard U . Bottom panels: Corresponding electronic compressibility. The Hund coupling strength has been set by keeping $J/U = 0.25$.

where U is the intraorbital Coulomb repulsion and J the Hund coupling [35]. In this framework the double counting energy for these interactions is absorbed into the chemical potential.

Here we solve the many-body Hamiltonian (2) within the slave-spin mean-field theory (SSMF) [36–38], which has proven to be a robust approximation for IBSC by, e.g., successfully capturing their orbital-differentiation signatures [20], or predicting the evolution of the Sommerfeld coefficient upon doping in the 122 family [7]. SSFMT describes the Fermi-liquid low-temperature paramagnetic metallic phase of (2) as a quasiparticle Hamiltonian

$$\hat{\mathcal{H}}_{\text{QP}} = \sum_{\substack{i \neq j \\ mm'\sigma}} \sqrt{Z_m Z_{m'}} t_{ij}^{mm'} \hat{f}_{im\sigma}^\dagger \hat{f}_{jm'\sigma} + \sum_{im\sigma} (\epsilon_m - \tilde{\lambda}_m) \hat{n}_{im\sigma}^f, \quad (3)$$

where the (orbital-dependent) quasiparticle renormalizations Z_m and on-site-energy shifts $\tilde{\lambda}_m$ are determined, solving the self-consistent slave-spin equations for given values of the local interactions U and J [38]. Further details on the solution of the SSMF equations can be found in the Supplemental Material [39].

In Fig. 3 we report the Sommerfeld coefficient as a function of the intraorbital Coulomb repulsion U , computed from the renormalized DoS in the case of LaFe_2As_2 , BaFe_2As_2 , and KFe_2As_2 . In the case of LaFe_2As_2 , we find that the experimental value is reproduced for local interactions of $U \approx 2.7 - 2.8$ eV and $J/U = 0.25$. Quite strikingly, these parameters are the same, capturing the evolution of the Sommerfeld coefficient along the $\text{K}_x\text{Ba}_{1-x}\text{Fe}_2\text{As}_2$ series, even accounting

for Rb and Cs substitutions [7], supporting the robustness of this model for the 122 family.

Such a finding naturally places LaFe_2As_2 in the realm of correlated metals, so questioning a pure interpretation of experimental findings in terms of effective doping of an uncorrelated band structure. In order to place LaFe_2As_2 within this framework, we report in Fig. 4 the mass renormalizations Z_m as a function of the interaction strength. As it appears from the top panels, LaFe_2As_2 displays a smoothed cross-over region similar to electron-overdoped ($n = 6.5/\text{Fe}$) BaFe_2As_2 , however, for the same value of the local interaction strength, the former is more correlated than the latter, with effective masses up to twice the PBE ones in the case of the xy orbitals. Considering that the same interaction strength has been used for both cases, such a behavior can be explained by the smaller bare bandwidth W of LaFe_2As_2 with respect to BaFe_2As_2 , so that a bigger U/W ratio is reached. Our model predicts therefore that LaFe_2As_2 is not electronically equivalent to BaFe_2As_2 with $n = 6.5 e^-/\text{Fe}$, but rather displays features which are compatible with an intermediate filling between $\text{BaFe}_2\text{As}_2(n = 6.5/\text{Fe})$ and $\text{BaFe}_2\text{As}_2(n = 6.0/\text{Fe})$. It must be stressed that this evolution is entirely due to dynamical correlation effects, and cannot therefore be captured by an independent-band model.

Such a doping evolution of electronic correlations has been shown to be an ubiquitous feature in IBSC, and reconciles several experimental observation within the $\text{K}_x\text{Ba}_{1-x}\text{Fe}_2\text{As}_2$ family [20]. Interestingly, the Hubbard-Kanamori Hamiltonian is believed to display a region of enhanced electronic compressibility $dn/d\mu$ in its (n, U) phase diagram, which

separates the normal metal from the Hund metal region [40,41]. It has also been recently speculated that the position of a material with respect to such an enhanced-compressibility region may be related to its superconducting critical temperature [42]. Inspection of the electronic compressibility, reported in the lower panels of Fig. 4, reveals that LaFe_2As_2 results closer to the enhancement region than electron-doped BaFe_2As_2 , further confirming the stronger degree of electronic correlations in the former, and possibly suggesting a key role of electronic correlations in the building of the IBSC superconducting state.

V. CONCLUSIONS

In conclusion, we have studied the electronic properties of LaFe_2As_2 by including electronic correlations in a realistic fashion by means of SSMF@DFT calculations. By leveraging on the numerical agility of our approach, we could freely explore the local interaction space and found that the experimental Sommerfeld coefficient is reproduced by

$U = 2.7 - 2.8$ eV and $J/U = 0.25$, the same values capturing its doping evolution across the $\text{K}_x\text{Ba}_{1-x}\text{Fe}_2\text{As}_2$ series. A comparison of the computed electronic properties between LaFe_2As_2 and the $\text{K}_x\text{Ba}_{1-x}\text{Fe}_2\text{As}_2$ series reveals that electronic correlations are stronger in LaFe_2As_2 for the same nominal filling of 6.5 electrons/Fe, due to the smaller bare bandwidth of the former. Our result points at the strength of electronic correlations, rather than sheer doping, as the key parameter in assessing the IBSC phase diagram.

ACKNOWLEDGMENTS

The authors acknowledge fruitful discussions with I. Pallecchi, M. Putti, and I. Timrov. T.G. and L.d.M. are supported by the European Commission through the ERC-CoG2016, StrongCoPhy4Energy, Grant Agreement No. 724177. This work was granted access to the HPC resources of MesoPSL financed by the Region Île-de-France and the project Equip@Meso (reference ANR-10-EQPX-29-01) of the programme Investissements d’Avenir, supervised by the Agence Nationale pour la Recherche.

-
- [1] D. C. Johnston, *Adv. Phys.* **59**, 803 (2010).
 - [2] P. D. Johnson, G. Xu, and W.-G. Yin, *Iron-Based Superconductivity*, Vol. 211 (Springer, 2015).
 - [3] A. Martinelli, F. Bernardini, and S. Massidda, *C. R. Phys.* **17**, 5 (2016).
 - [4] G. R. Stewart, *Rev. Mod. Phys.* **83**, 1589 (2011).
 - [5] P. Dai, *Rev. Mod. Phys.* **87**, 855 (2015).
 - [6] F. Hardy, P. Burger, T. Wolf, R. Fisher, P. Schweiss, P. Adelman, R. Heid, R. Fromknecht, R. Eder, D. Ernst *et al.*, *EPL (Europhysics Letters)* **91**, 47008 (2010).
 - [7] F. Hardy, A. E. Böhmer, L. de’ Medici, M. Capone, G. Giovannetti, R. Eder, L. Wang, M. He, T. Wolf, P. Schweiss, R. Heid, A. Herbig, P. Adelman, R. A. Fisher, and C. Meingast, *Phys. Rev. B* **94**, 205113 (2016).
 - [8] A. Iyo, K. Kawashima, S. Ishida, H. Fujihisa, Y. Gotoh, H. Eisaki, and Y. Yoshida, *J. Am. Chem. Soc.* **140**, 369 (2018).
 - [9] A. Iyo, S. Ishida, H. Fujihisa, Y. Gotoh, I. Hase, Y. Yoshida, H. Eisaki, and K. Kawashima, *J. Phys. Chem. Lett.* **10**, 1018 (2019).
 - [10] H. Usui and K. Kuroki, *Phys. Rev. Res.* **1**, 033025 (2019).
 - [11] I. I. Mazin, M. Shimizu, N. Takemori, and H. O. Jeschke, *Phys. Rev. Lett.* **123**, 267001 (2019).
 - [12] A. I. Coldea, J. D. Fletcher, A. Carrington, J. G. Analytis, A. F. Bangura, J.-H. Chu, A. S. Erickson, I. R. Fisher, N. E. Hussey, and R. D. McDonald, *Phys. Rev. Lett.* **101**, 216402 (2008).
 - [13] V. Brouet, M. Marsi, B. Mansart, A. Nicolaou, A. Taleb-Ibrahimi, P. Le Fevre, F. Bertran, F. Rullier-Albenque, A. Forget, and D. Colson, *Phys. Rev. B* **80**, 165115 (2009).
 - [14] G. Lee, H. S. Ji, Y. Kim, C. Kim, K. Haule, G. Kotliar, B. Lee, S. Khim, K. H. Kim, K. S. Kim *et al.*, *Phys. Rev. Lett.* **109**, 177001 (2012).
 - [15] T. Terashima, N. Kurita, M. Kimata, M. Tomita, S. Tsuchiya, H. Satsukawa, A. Harada, K. Hazama, M. Imai, A. Sato *et al.*, *J. Phys.: Conf. Ser.* **449**, 012022 (2013).
 - [16] M. D. Watson, T. K. Kim, A. A. Haghighirad, N. R. Davies, A. McCollam, A. Narayanan, S. F. Blake, Y. L. Chen, S. Ghannadzadeh, A. J. Schofield, M. Hoesch, C. Meingast, T. Wolf, and A. I. Coldea, *Phys. Rev. B* **91**, 155106 (2015).
 - [17] T. Kouchi, M. Yashima, H. Mukuda, S. Ishida, H. Eisaki, Y. Yoshida, K. Kawashima, and A. Iyo, *J. Phys. Soc. Jpn.* **88**, 113702 (2019).
 - [18] I. Pallecchi, A. Iyo, H. Ogino, M. Affronte, and M. Putti, *Phys. Rev. Mater.* **4**, 114803 (2020).
 - [19] Z. Yin, K. Haule, and G. Kotliar, *Nat. Mater.* **10**, 932 (2011).
 - [20] L. de’ Medici, G. Giovannetti, and M. Capone, *Phys. Rev. Lett.* **112**, 177001 (2014).
 - [21] T. Gorni, P. Villar Arribi, M. Casula, and L. de’ Medici, *Phys. Rev. B* **104**, 014507 (2021).
 - [22] S. Acharya, D. Pashov, F. Jamet, and M. van Schilfgaarde, *Phys. Rev. Lett.* **124**, 237001 (2020).
 - [23] J. Zhao, Y. Wang, X. Feng, and S. A. Yang, *Phys. Rev. B* **103**, 125125 (2021).
 - [24] P. Giannozzi, S. Baroni, N. Bonini, M. Calandra, R. Car, C. Cavazzoni, D. Ceresoli, G. Chiarotti, M. Cococcioni, I. Dabo, A. Dal Corso, S. De Gironcoli, S. Fabris, G. Fratesi, R. Gebauer, U. Gerstmann, C. Gougoussis, A. Kokalj, M. Lazzeri, L. Martin-Samos, N. Marzari, F. Mauri, R. Mazzarello, S. Paolini, A. Pasquarello, L. Paulatto, C. Sbraccia, S. Scandolo, G. Schlauser, A. Seitonen, A. Smogunov, P. Umari, and R. Wentzcovitch, *J. Phys.: Condens. Matter* **21**, 395502 (2009).
 - [25] P. Giannozzi, O. Andreussi, T. Brumme, O. Bunau, M. Buongiorno Nardelli, M. Calandra, R. Car, C. Cavazzoni, D. Ceresoli, M. Cococcioni, N. Colonna, I. Carnimeo, A. Dal Corso, S. de Gironcoli, P. Delugas, R. A. DiStasio Jr., A. Ferretti, A. Floris, G. Fratesi, G. Fugallo, R. Gebauer, U. Gerstmann, F. Giustino, T. Gorni, J. Jia, M. Kawamura, H.-Y. Ko, A. Kokalj, E. Küçükbenli, M. Lazzeri, M. Marsili, N. Marzari, F. Mauri, N. L. Nguyen, H.-V. Nguyen, A. Otero-de-la Rosa, L. Paulatto, S. Poncé, D. Rocca, R. Sabatini,

- B. Santra, M. Schlipf, A. Seitsonen, A. Smogunov, I. Timrov, T. Thonhauser, P. Umari, N. Vast, and S. Baroni, *J. Phys.: Condens. Matter* **29**, 465901 (2017).
- [26] M. van Setten, M. Giantomassi, E. Bousquet, M. Verstraete, D. Hamann, X. Gonze, and G.-M. Rignanesse, *Comput. Phys. Commun.* **226**, 39 (2018).
- [27] P. Villar Arribi, Heavy fermions and Hund's metals in iron-based superconductors, Ph.D. thesis, Université Grenoble Alpes, 2018, https://theses.hal.science/tel-02151075/file/VILLAR-ARRIBI_2018_archivage.pdf.
- [28] As routinely done in planewave+pseudopotential codes, atomic wavefunctions are obtained via a Löwdin orthogonalization of the pseudopotential atomic eigenstates [29].
- [29] D. Sanchez-Portal, E. Artacho, and J. M. Soler, *Solid State Commun.* **95**, 685 (1995).
- [30] G. Pizzi, V. Vitale, R. Arita, S. Blügel, F. Freimuth, G. Géranton, M. Gibertini, D. Gresch, C. Johnson, T. Koretsune *et al.*, *J. Phys.: Condens. Matter* **32**, 165902 (2020).
- [31] N. Marzari, A. A. Mostofi, J. R. Yates, I. Souza, and D. Vanderbilt, *Rev. Mod. Phys.* **84**, 1419 (2012).
- [32] I. Souza, N. Marzari, and D. Vanderbilt, *Phys. Rev. B* **65**, 035109 (2001).
- [33] T. Miyake, K. Nakamura, R. Arita, and M. Imada, *J. Phys. Soc. Jpn.* **79**, 044705 (2010).
- [34] S. Graser, A. F. Kemper, T. A. Maier, H.-P. Cheng, P. J. Hirschfeld, and D. J. Scalapino, *Phys. Rev. B* **81**, 214503 (2010).
- [35] Here the local off-diagonal terms of the Kanamori Hamiltonian (spin-flip and pair-hopping) are customarily dropped.
- [36] L. de' Medici, A. Georges, and S. Biermann, *Phys. Rev. B* **72**, 205124 (2005).
- [37] S. R. Hassan and L. de' Medici, *Phys. Rev. B* **81**, 035106 (2010).
- [38] L. de' Medici and M. Capone, *The Iron Pnictide Superconductors* (Springer, 2017), pp. 115–185.
- [39] See Supplemental Material at <http://link.aps.org/supplemental/10.1103/PhysRevB.107.125166> for further details on our tight-binding d models.
- [40] L. de' Medici, *Phys. Rev. Lett.* **118**, 167003 (2017).
- [41] M. Chatzieftheriou, M. Berović, P. V. Arribi, M. Capone, and L. de' Medici, *Phys. Rev. B* **102**, 205127 (2020).
- [42] P. Villar Arribi and L. de' Medici, *Phys. Rev. Lett.* **121**, 197001 (2018).